Journal of Materials Chemistry A

ROYAL SOCIETY OF CHEMISTRY

REVIEW

View Article Online
View Journal | View Issue

Check for updates

Cite this: J. Mater. Chem. A, 2023, 11, 5460

Adsorption-based capture of iodine and organic iodides: status and challenges

Tingting Pan, Kaijie Yang, Xinglong Dong and Yu Han *

Nuclear energy is a sustainable low-carbon energy source that plays an increasingly important role in supporting the progress of human society. However, there are safety issues associated with the operation of nuclear reactors. In particular, volatile radioactive elements, primarily ^{129}I and ^{131}I, in the form of molecular iodine (I_2) or organic iodides (*e.g.*, CH_3I and CH_3CH_2I), are harmful for the environment and human health and must be removed before discharging the off-gas. Adsorption processes employing porous solid adsorbents to capture radioactive iodine compounds have attracted considerable attention owing to their simple operation and low maintenance cost and because they avoid the use of highly corrosive solutions. Despite the efforts devoted to developing novel adsorbents for iodine capture, certain critical issues related to practical applications have been overlooked. This review summarizes the adsorption mechanisms employed to capture I_2 and CH_3I, focusing on the different adsorbent requirements. This review also compares the static and dynamic evaluation systems, analyzes the structure–function relationship under different testing conditions, and highlights the importance of using appropriate conditions to evaluate adsorbents. Moreover, the simultaneous capture of I_2 and CH_3I is discussed, which is quite challenging but has been largely ignored in previous studies. Finally, this review outlines the challenges and opportunities in this field from the perspective of materials design and system evaluation, indicating that properly designing adsorbents to provide sufficient chemisorption sites may be the only way to meet the practical application requirements.

Received 5th December 2022
Accepted 23rd February 2023

DOI: 10.1039/d2ta09448g

rsc.li/materials-a

Open Access Article. Published on 24 2023. Downloaded on 23.04.26 04:24:07.
This article is licensed under a Creative Commons Attribution-NonCommercial 3.0 Unported Licence.

1. Introduction

Nuclear power is one of the most important low-carbon energy sources, which is used to currently generate ~10% of the global electricity.[1] However, the reprocessing of used fuel rods or severe nuclear accidents can produce radioactive gaseous fission products such as $^{129/131}I$, ^{127}Xe, and ^{85}Kr.[2–4] Therefore, technologies are required to efficiently capture these radioactive wastes, particularly iodine, because of its high volatility and well-established adverse effects on human health. Among the iodine radioisotopes, ^{129}I has an extremely long half-life of 15.7 $\times$ 10^6 years and a lasting environmental impact. Although ^{131}I has a relatively short half-life (approximately eight days), it requires to be immediately captured upon its release because it can damage the thyroid and interfere with the human metabolic process.[5,6] The common forms of radioactive iodine in the off-gases of nuclear power plants include molecular iodine (I_2), organic iodides such as methyl iodide (CH_3I) and ethyl iodide (CH_3CH_2I). Inorganic radioactive iodine-containing compounds, such as HI, HOI, and ICN, may also be present, but usually in vary small amounts.[7–10] Because of the different physicochemical properties of molecular iodine and organic iodides, specially designed absorption or adsorption systems are needed to achieve the desired capture efficiency and capacity.

Liquid scrubbing processes have been used to capture radioactive I_2 and other I-containing compounds from the off-gas, requiring highly corrosive solutions and high maintenance costs.[11] Therefore, adsorption-based radioiodine capture has attracted considerable attention (Fig. 1). Activated carbon and

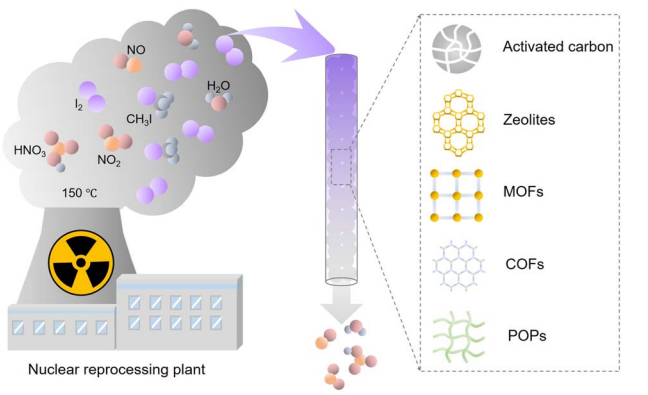

Fig. 1 Schematic of the components in nuclear off-gas generated during the reprocessing process and emerging iodine adsorbents.

Advanced Membranes and Porous Materials (AMPM) Center, Physical Sciences and Engineering Division, King Abdullah University of Science and Technology (KAUST), Thuwal, 23955-6900, Saudi Arabia. E-mail: yu.han@kaust.edu.sa

This journal is © The Royal Society of Chemistry 2023

Open Access Article. Published on 24 2023. Downloaded on 23.04.26 04:24:07.
This article is licensed under a Creative Commons Attribution-NonCommercial 3.0 Unported Licence.

zeolite materials are the most popular industrial adsorbents, but they have low adsorption capacities for iodine and organic iodides. Hence, they cannot meet the requirements of practical applications.[12–15] Emerging porous materials, such as metal organic frameworks (MOFs),[16–20] porous organic polymers (POPs),[21–26] and covalent organic frameworks (COFs),[27–29] provide new platforms for developing high-performance adsorbents because of their diverse structures, large surface areas, tunable pore sizes, and designable surface functionalities. Many studies have examined iodine capture based on these emerging adsorbent materials.[30–32] However, the conditions most studies used to evaluate adsorbents were not related to practical applications. In particular, many studies measured the I_2 adsorption capacity of the developed adsorbents using saturated I_2 vapor, ignoring that the actual concentration of I_2 in the off-gas stream is orders of magnitude lower. Furthermore, most studies have focused only on the I_2 adsorption and ignored the coexisting organic iodides. Adsorbents are difficult to assess without standardizing the measurement conditions because the adsorption capacity is closely related to the type and concentration of the adsorbate. Moreover, although multiple review articles have summarized the adsorption capacities of various reported adsorbent materials, there has been no systematic analysis of the differences in the adsorption mechanism of iodine and organic iodides.

This review article differs from the previous ones in the following ways. First, this article is structured based on the adsorption mechanism rather than the material type, in which iodine adsorption and organic iodide adsorption are separately discussed because of their different requirements for the adsorbent. Second, this article critically points out that the experimental conditions used in most studies were different from actual off-gas treatment applications and analyzes the origin of unreasonably high I_2 adsorption capacities reported in the literature. Third, this article highlights the importance of evaluating adsorbent materials for simultaneous capture of iodine and organic iodides at low concentrations (<150 ppmv), high temperatures (~150 °C), and dynamic conditions, which has largely been overlooked in previous original research and review articles. Lastly, this article discusses the challenges and future opportunities in this field from material design and performance evaluation perspectives.

2. Mechanisms for molecular iodine capture

Molecular iodine is the primary component of radioactive iodine species in off-gas, which can be captured chemically or physically using various mechanisms, including redox reactions, coordination interactions, electrophilic aromatic substitution, Lewis acid–base interactions, Coulomb interactions, hydrogen bonding, van der Waals interactions, and hydrophobic interactions.

2.1 Redox reactions

Metal-containing adsorbents can capture I_2 *via* redox reactions. Ag is the most commonly used metal because it can specifically react with I_2. Among the various support materials,[13–15] zeolites are used widely because of their ion-exchange ability and inherent porosity, allowing for the easy loading and high dispersion of silver. The capture of I_2 by Ag-zeolites involves the following reactions, depending on the state of Ag:[33]

$$I_2 + 2Ag^0 \rightarrow 2AgI \quad (1)$$

$$I_2 + 2Ag^+ + H_2O \rightarrow AgI + AgIO + 2H^+ \quad (2)$$

$$AgIO + O_2 \rightarrow AgIO_3 \quad (3)$$

The standard practice is to reduce the Ag species on the adsorbent to Ag^0 prior to use for I_2 capture, and studies have been performed to understand the respective roles of Ag^0 and Ag^+ in this process. For example, Nenoff *et al.* examined the distribution and structure of AgI formed in the Ag-MOR zeolite using a differential pair distribution function method.[34] They reported that for reduced Ag-MOR (Ag^0-MOR), two AgI phases are formed after I_2 capture, *i.e.*, α-AgI clusters in the zeolite pores and γ-AgI nanoparticles on the surface. For unreduced Ag-MOR (Ag^+-MOR), all formed AgI was confined within the pores as α-AgI clusters (Fig. 2a). These results suggest that Ag^+-MOR is superior to Ag^0-MOR for the long-term storage of I_2 because it can trap all captured I_2 in the zeolite pores.

In addition to Ag^+ and Ag^0, Ag_2O can capture I_2.[35,36] However, the reactivity of Ag_2O towards I_2 is controversial. Nan *et al.* suggested that the decreased adsorption capacity of Ag^0-MOR above 150 °C in the presence of water is associated with the oxidation of Ag^0 to Ag_2O or AgOH.[15] Holladay *et al.* attributed the adverse effects of NO_2 on I_2 adsorption to it slowly oxidizing Ag^0 in Ag^0-MOR.[37] In general, the primary advantage of Ag-zeolites compared to other adsorbents for I_2 capture is their high capacity at high temperatures because of the chemical reaction-based capture mechanism. Nevertheless, Ag-zeolites have limitations such as high cost and potential environmental toxicity.

Other metals have been assessed as alternatives to Ag for I_2 capture. Huve *et al.* compared the Gibbs free energies of iodides and oxides of different metals (Ag, Cu, Hg, Fe, Tl, Sn, Cd, Pb, and Ti). They reported that oxides form preferentially over halides for all metals except Ag and Hg.[38] In recent years, Bi-

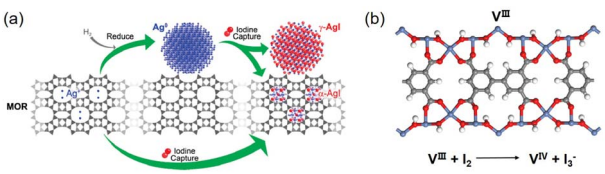

Fig. 2 (a) Schematic of the I_2 capture process using Ag-MOR zeolite as the adsorbent. For Ag^0 sites, I_2 adsorption leads to the formation of two AgI phases, *i.e.*, α-AgI clusters in the zeolite pores and γ-AgI nanoparticles on the zeolite surface. For Ag^+ sites, only α-AgI clusters are formed in the pores. Reproduced with permission from ref. 34. Copyright 2010, American Chemical Society. (b) Structure model of MOF MFM-300(V^{III}) and the redox reaction upon I_2 adsorption. Color code: blue, V^{III}; red, O; gray, C; white, H.[43]

Open Access Article. Published on 24 2023. Downloaded on 23.04.26 04:24:07.
This article is licensed under a Creative Commons Attribution-NonCommercial 3.0 Unported Licence.

based materials are becoming promising alternatives to Ag-based adsorbents because they incur lower production costs while maintaining high I_2 capture capacity.[39–41] The reactions of Bi with I_2 are as follows:

$$Bi + 1.5I_2 \rightarrow BiI_3 \quad (4)$$

$$2BiI_3 + O_2 \rightarrow 2BiOI + 2I_2 \quad (5)$$

$$5BiOI + O_2 \rightarrow Bi_5O_7I + 2I_2 \quad (6)$$

Yim *et al.* used thiol-functionalized mesoporous silica SBA-15 to immobilize Bi for capturing I_2 vapor.[39] The prepared Bi-SBA-15 outperformed Ag-zeolites in terms of I_2 uptake capacity at 150 °C. However, as the temperature was increased to 250 °C, the I_2 uptake of Bi-SBA-15 sharply decreased to ~50% of Ag-X zeolite.[42] This reversal in adsorption capacity may be attributed to two reasons. The chemical bond between bismuth and sulfur is less stable than that between Ag and zeolite, which breaks at 250 °C. Moreover, the Gibbs free energy of BiI_3 is less than that of AgI at high temperatures.

Metal sites in redox-active MOFs can capture I_2 *via* redox reactions. Schröder *et al.* examined the forms of adsorbed iodine in MFM-300(V^{III}) and its oxidized analogue, MFM-300(V^{IV}).[43] A redox reaction occurred when MFM-300(V^{III}) was used as the adsorbent, as evidenced by the generation of I_3^- and V^{IV} (Fig. 2b). However, I_2 was only physically adsorbed when MFM-300 (V^{IV}) was used as the adsorbent because the high-valence metal sites (V^{IV}) could not be oxidized. In this study, the difference in the I_2 adsorption capacity between the two adsorbents was insignificant because, under the measurement conditions used (343 K; high I_2 concentrations), the I_2 uptake was primarily determined by the pore volume of the adsorbent rather than the adsorbent/adsorbate interaction strength.

2.2 Coordination interactions

In addition to redox reactions, the metal sites in adsorbents can capture I_2 *via* coordination interactions if they are coordinately unsaturated. For example, Baladi *et al.* reported that polymers containing three-coordinated Cu^+ are favorable for I_2 adsorption, while those with similar structures but with four-coordinated Cu^+ barely adsorb I_2.[44] Similarly, coordinately unsaturated (open) metal sites in MOF materials have been used for I_2 capture. The MOF Co_2(*p*-DOBDC) (*p*-DOBDC^{4-} = 2,5-dioxo-1,4-benzenedicarboxylate) has open Co sites that can adsorb I_2 in an end-on configuration with a Co–I–I angle of 123°, as determined *via* single-crystal X-ray diffraction (SXRD) (Fig. 3a).[45] As per the studies of the I_2 coordination behaviors in organometallics, I_2 can act as a donor or an acceptor, depending on the nature of the metal center.[46] When I_2 acts as the acceptor, it bonds with the metal center collinearly using the σ*(I–I) orbital as the acceptor orbital. When I_2 acts as the donor, it exhibits a bent coordination bond with the metal center using a p-type lone pair localized on one of the two iodine atoms as a dominant donation. For I_2-loaded Co_2(*p*-DOBDC), the determined bond angle suggested that I_2 acted as the donor while the open Co sites acted as acceptors.

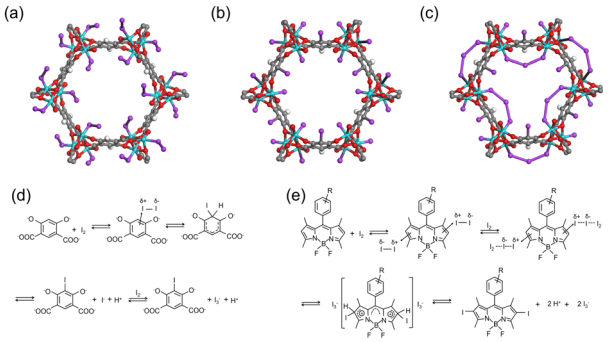

Fig. 3 (a) Structure of Co_2(*p*-DOBDC) (*p*-DOBDC^{4-} = 2,5-dioxo-1,4-benzenedicarboxylate) with 10% I_2 loading, where I_2 coordinately interacts with open Co sites in an end-on configuration. Reproduced with permission from ref. 45. Copyright 2019, American Chemical Society. (b and c) Structures of Co_2(*m*-DOBDC) (*m*-DOBDC^{4-} = 4,6-dioxo-1,3-benzenedicarboxylate) with 10 wt% (b) and 100 wt% (c) I_2 loading. Reproduced with permission from ref. 45. Copyright 2019, American Chemical Society. At 10 wt% I_2 loading, *m*-DOBDC chemically adsorb I_2 *via* an electrophilic aromatic substitution reaction, with the remaining I^- coordinated to the open Co site. At 100% I_2 loading, additional I_2 coordinates with residual open Co sites and bridges the neighboring I^-, forming triiodides (I_3^-). (d) Scheme of the electrophilic aromatic substitution reaction between I_2 and *m*-DOBDC^{4-}. Reproduced with permission from ref. 45. Copyright 2019, American Chemical Society. (e) A reaction mechanism proposed for the iodination reaction between I_2 and 2,6 position of BODIPY (4,4-difluoro-4-bora-3a,4a-diaza-*s*-indacene). Reproduced with permission from ref. 49. Copyright 2013, Royal Society of Chemistry. Color code: cyan, Co; red, O; purple, I; gray, C; white, H.

Because the real-world nuclear off-gas contains a considerable amount of water, Nenoff *et al.* examined the I_2 adsorption behavior of HKUST-1 using a mixture of I_2 and H_2O.[47] They reported that the coordinated water molecules impede the direct interaction of I_2 with the open sites, and these water molecules "hold" I_2 molecules *via* weak interactions with I···O distances of 3.46–3.84 Å. The adsorbed I_2 molecules form a hydrophobic barrier that minimizes H_2O sorption. To summarize, HKUST-1 exhibits an I_2/H_2O selectivity of 1.5 when considering the same concentrations of I_2 and H_2O in the mixture.

2.3 Electrophilic aromatic substitution

Electrophilic aromatic substitution reactions involve the replacement of a hydrogen atom on a benzene ring with an electrophile. As an electrophile, I_2 can be captured by adsorbents containing suitable functional groups *via* such reactions, where the substituent groups on the aromatic ring directly affect the reactive site. For example, when the MOF Co_2(*m*-DOBDC) (*m*-DOBDC^{4-} = 4,6-dioxo-1,3-benzenedicarboxylate) was used to capture I_2, in addition to the Co sites, the organic linker *m*-DOBDC could adsorb I_2 chemically *via* an electrophilic aromatic substitution reaction (Fig. 3b).[45] However, the organic linker in Co_2(*p*-DOBDC) could not react with I_2 (Fig. 3a) because the different distribution of substituent groups results in different reactivity, *i.e.*, *m*-DOBDC is more electron-rich at the fifth position of the benzene ring than *p*-DOBDC.

 This journal is © The Royal Society of Chemistry 2023

Open Access Article. Published on 24 2023. Downloaded on 23.04.26 04:24:07.
This article is licensed under a Creative Commons Attribution-NonCommercial 3.0 Unported Licence.

During I_2 adsorption on Co_2(*m*-DOBDC), the open Co sites and electron-rich ligands cooperatively polarize I_2 to the [$I^{\delta+}$–$I^{\delta-}$] state at a low I_2 loading. Subsequently, the aryl C5–H bond reacts with $I^{\delta+}$ to form a C–I bond, and the remaining I^- coordinated to the open Co site (Fig. 3b and d).[45] At a higher I_2 loading, additional I_2 coordinates with the residual open Co sites and bridges the neighboring I^-, thus forming triiodides (I_3^-) (Fig. 3c).

The 2,6-positions of 4,4-difluoro-4-bora-3a,4a-diaza-*s*-indacene (BODIPY) bearing a lower positive charge can undergo rapid iodination when exposed to I_2 at room temperature (Fig. 3e).[48] Therefore, Zhu *et al.* synthesized two BODIPY based conjugated porous polymers, BDP-CPP-1 and BDP-CPP-2.[49] They hypothesized that in BDP-CPP-2, ethyl groups were substituted at the 2,6-positions of BODIPY, therefore these positions were not useful for electrophilic aromatic substitution. They observed that BDP-CPP-1 could adsorb additional I_2 than BDP-CPP-2 (2.83 *vs.* 2.23 g g^{-1}) and attributed this to the additional adsorption capacity of BDP-CPP-1 associated with electrophilic aromatic substitution. However, they ignored the difference in the number of functional groups per unit mass between the two polymers.

Although chemisorption based on covalent C–I bond formation prevents the release of adsorbed I_2, it poses challenges to the regeneration of the organic adsorbent. In contrast, inorganic adsorbents that chemisorb I_2 by forming AgI can be regenerated *via* calcination in a reducing atmosphere.[50]

2.4 Lewis acid–base interactions

Molecular iodine is widely used as a mild Lewis acid catalyst for various organic reactions. Therefore, I_2 capture can be achieved using adsorbents with basic groups *via* Lewis acid–base interactions.[51] Neutral charge-transfer complexes (D·I_2) or charged polyiodides, such as I_3^- and I_5^-, can be generated depending on the donor ability of the Lewis bases (D).[52]

X-ray photoelectron spectroscopy (XPS) and Raman spectroscopy are the most commonly used characterization tools for identifying the formed iodine species. However, the assignments of the XPS peaks for different iodine species (I_2, I_3^- and I_5^-) are inconsistent in the literature. For example, peaks at 630.2 and 618.6 eV were assigned to I_2 in certain studies[49,53,54] but to I_3^- in others.[55,56] By comparison, Raman spectroscopy is a more reliable approach for distinguishing the formed iodine species. When neutral D·I_2 complexes are formed, the characteristic Raman band of solid I_2 at 180 cm^{-1} is expected to move toward a lower frequency (Fig. 4a). When charged polyiodides are formed, I_3^- exhibits a symmetric stretching band at ~110 cm^{-1} and an asymmetric stretching band at ~140 cm^{-1}, while the band around 160 cm^{-1} is usually assigned to I_5^- species (Fig. 4b).[57]

Although the generation of negatively charged polyiodides is generally accepted, there is no consensus on the species balancing of these negative charges. In previous studies, positively charged species, such as $(D–I)^+$ (Fig. 4c)[58–60] and D_2^+ (Fig. 4d),[61,62] were proposed as counter cations.

The Lewis basic sites commonly incorporated into adsorbents for I_2 capture can be divided into different categories (see Fig. 5), which are separately discussed below.

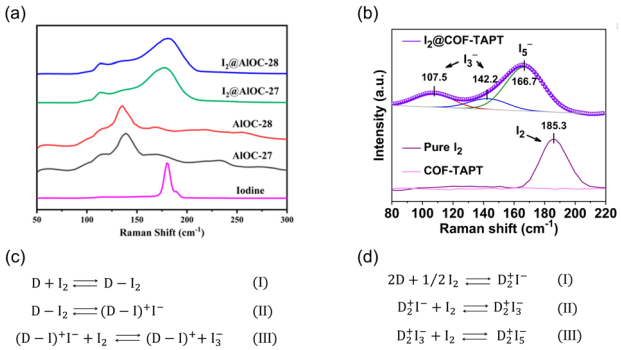

Fig. 4 (a) Raman spectra of AlOC-27, AlOC-28, I_2@AlOC-27-NC, I_2@AlOC-28-NC, and solid I_2. In the spectra of I_2@AlOC-27-NC and I_2@AlOC-28-NC, the peak at 180 cm^{-1} assigned to solid I_2 was red-shifted, indicating the formation of neutral charge transfer complex D·I_2. Reproduced with permission from ref. 73. Copyright 2021, American Chemical Society. (b) Raman spectra of pure I_2, pristine COF-TAPT, and I_2-saturated COF-TAPT. In the spectra of I_2@COF-TAPT, peaks attributed to I_3^- and I_5^- appeared, indicating the formation of charged polyiodides in COF-TAPT. Reproduced with permission from ref. 99. Copyright 2022, Springer Nature. (c and d) The interaction mechanisms between electron donors and I_2 proposed by different researchers.[58–62]

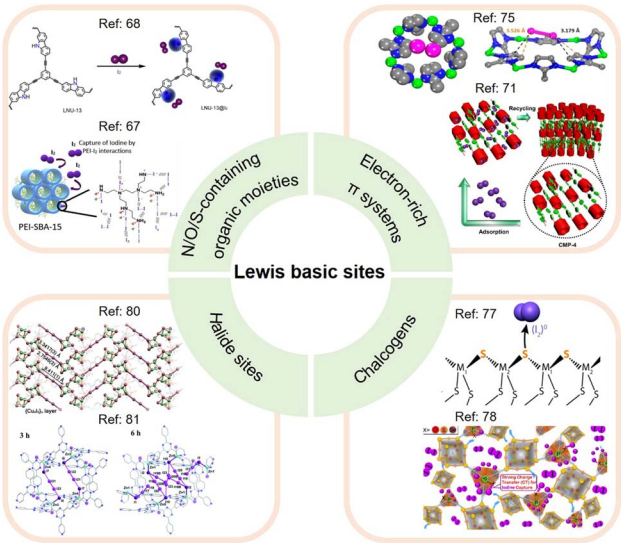

Fig. 5 Classification of Lewis basic sites used for I_2 capture, including N/O/S-containing organic moieties, electron-rich π systems, chalcogens, and halide sites. (Top left panel) The upper figure is reproduced with permission from ref. 68. Copyright 2021, MDPI. The lower figure is reproduced with permission from ref. 67. Copyright 2019, Elsevier. (Top right panel) The upper figure is reproduced with permission from ref. 75. Copyright 2013, American Chemical Society. The lower figure is reproduced with permission from ref. 71. Copyright 2021, Wiley. (Bottom right panel) The upper figure is reproduced with permission from ref. 77. Copyright 2013, American Chemical Society. The lower figure is reproduced with permission from ref. 78. Copyright 2020, Elsevier. (Bottom left panel) The upper figure is reproduced with permission from ref. 80. Copyright 2017, Wiley. The lower figure is reproduced from ref. 81 with permission from the Royal Society of Chemistry.

Open Access Article. Published on 24 2023. Downloaded on 23.04.26 04:24:07.
This article is licensed under a Creative Commons Attribution-NonCommercial 3.0 Unported Licence.

2.4.1 N/O/S-containing organic moieties. Organic moieties containing N/S/O heteroatoms can be incorporated into adsorbents to improve their I_2 adsorption capacities. The heteroatom lone-pair electrons are transferred to the antibonding orbital (σ^*) of I_2, thus forming charge-transfer complexes. This strategy has often been used in porous organic polymers (POPs) because their flexible structures can easily incorporate functional groups containing heteroatoms.[63–68] For example, Jiang *et al.* synthesized a number of COFs containing abundant tertiary amine active sites.[69] Owing to the high density of N sites, these COFs could efficiently capture iodine with the optimal adsorption capacity reaching 5.54 g g^{-1}. The adsorption strength was regulated by introducing different functional groups into the structure. Among the materials investigated, COF TAPD-DMTA with electron-donating methoxy groups demonstrated the highest binding energy with I_2 (−17.32 kcal mol^{-1}). However, COF TAPD-DHTA with hydroxyl groups had the lowest binding energy (−14.91 kcal mol^{-1}) because hydroxyl groups tend to form an intramolecular hydrogen bond with N active sites, thus resulting in a lower electron cloud density.

2.4.2 Electron-rich π systems. Organic moieties containing localized or conjugated π electrons, such as double bonds, triple bonds, benzene rings, and other aromatic conjugated structures, have been demonstrated to help promote I_2 adsorption.[70–73] The promotion effect is based on the Lewis acid–base interactions between the π electrons of the adsorbent and the σ^* orbital of I_2. Porous aromatic frameworks (PAF-23, PAF-24, and PAF-25) incorporating ionic bonds, phenyl rings, and triple bonds exhibited high I_2 adsorption capacity.[74] As a control sample, PAF-21, structurally similar to PAF-23 but without triple bonds, was synthesized and assessed for I_2 adsorption. PAF-21 had a considerably lower I_2 uptake than PAF-23 (1.52 *vs.* 2.71 g g^{-1}), indicating the important role of π-electron donors in promoting I_2 adsorption.

Moreover, the pore geometry of the adsorbent material affects the distribution of adsorption sites and thus the binding strength to I_2. For example, Nenoff *et al.* reported that each I_2 molecule adsorbed in MOF ZIF-8 simultaneously interacts with two opposing 2-methylimidazolate linkers to form an iodine-aromatic charge-transfer complex because of the special pore size and shape of ZIF-8.[75] The consequence of such multiple interactions is that ZIF-8 can firmly trap the adsorbed I_2 until the framework decomposes at ~575 K.[76]

2.4.3 Chalcogens. Usually, chalcogens (S, Se, and Te) are incorporated into aerogels to form chalcogels for I_2 capture. Riley *et al.* fabricated various chalcogels ($Co_{0.7}Bi_{0.3}MoS_4$, $Co_{0.7}Cr_{0.3}MoS_4$, $Co_{0.5}Ni_{0.5}MoS_4$, $PtGe_2S_5$, and Sn_2S_3) and examined their I_2 adsorption capability.[77] Under their testing conditions, all chalcogels exhibited > 99.0% I_2 capture efficiency. The electron-donating property of chalcogens can be enhanced by designing the surrounding chemical environment. For example, a polymeric adsorbent for I_2 capture was prepared, in which phosphine chalcogenide ligands, P = X (X refers to O, S, and Se) could transfer π-electrons from adjacent aromatic rings to the captured I_2, thereby increasing the interaction strength.[78] Consequently, the as-prepared polymer, POSS-TPPX, captured a considerable amount of I_2 (0.26 g g^{-1}) even at a high temperature of 160 °C and an extremely low I_2 concentration of 0.16 ppmv.

2.4.4 Halide sites. Halide sites are electron-rich and can act as Lewis bases to facilitate I_2 adsorption.[79,80] Brunet *et al.* examined the I_2 adsorption on a porous MOF ($[[(ZnI_2)_3(TPT)_2 \cdot 5.5(C_6H_5NO_2)]_n$), in which iodides were attached to Zn to form metal iodide sites.[81] Single-crystal X-ray crystallography showed that the guest I_2 molecules were initially bound with two terminal iodides in the framework to form $[I_4]^{2-}$ units. As adsorption progressed, each $[I_4]^{2-}$ unit was converted to two less energetically favorable I_3^- groups to accommodate additional I_2 molecules.

2.5 Coulomb interactions

Another effective strategy to promote I_2 adsorption is to generate ionic sites in the adsorbent, which can bind the dynamically formed polyiodide anions *via* Coulomb interactions.[21,74,82] However, despite the enhanced affinity to I_2, the generation of ionic sites in various amorphous POPs *via* post-synthesis modification usually leads to a greatly reduced surface area and limited improvement in the I_2 adsorption capacity. Xie *et al.* introduced ionic sites into crystalline COFs using a "multivariate" strategy combined with a post-synthesis modification to overcome this issue.[83] The as-prepared ionic COF (iCOF-AB-50) combined large surface areas, high pore volume, and abundant binding sites, resulting in excellent I_2 capture performance under dynamic conditions (279 wt% at 25 °C). In particular, the significant promoting effect of the introduced ionic groups (quaternary ammonium) was attributed to their strong interactions with $[I_2Br]^-$ and $[2I_2Br]^-$ species *via* Coulomb forces.[83]

A highly stable ionic guanidinium-based COF (TGDM) was developed recently (Fig. 6).[84] TGDM has a high density of robust ionic sites owing to the reduced linker length and the unique stability of the guanidium moieties, which makes it particularly useful for I_2 capture at high temperatures. At 150 °C and 150 ppmv of I_2, TGDM exhibited an I_2 adsorption capacity of ~30 wt%, which was considerably higher than that of multiple benchmark adsorbents.

2.6 Hydrogen bonding

Hydrogen bonding has been used to facilitate I_2 adsorption. The polyiodide I_3^- is readily formed in multiple adsorbents, which

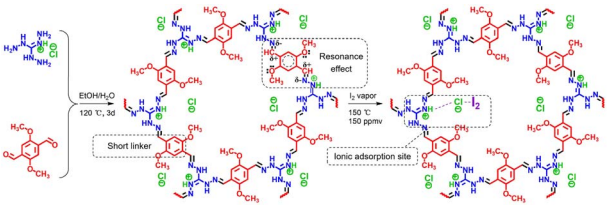

Fig. 6 Schematic of the design and synthesis of ionic COF TGDM and explanation of its high stability and I_2 uptake mechanism. Reproduced with permission from ref. 84. Copyright 2022, American Chemical Society. The ionic sites (quaternary ammonium) strongly interact with $[I_2Cl]^-$ species through Coulomb forces.

This journal is © The Royal Society of Chemistry 2023

Open Access Article. Published on 24 2023. Downloaded on 23.04.26 04:24:07.
This article is licensed under a Creative Commons Attribution-NonCommercial 3.0 Unported Licence.

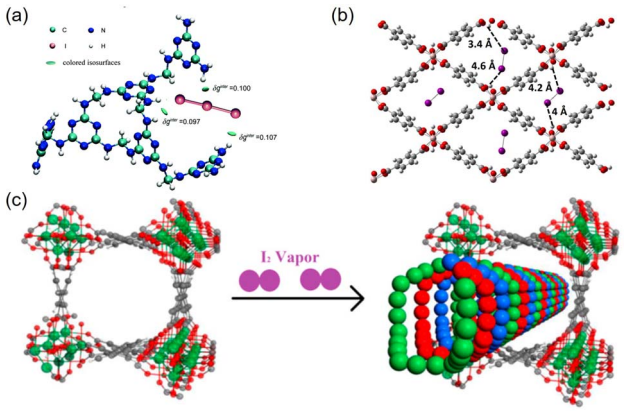

Fig. 7 (a) DFT-calculated hexamer model of MFP bound with I_3^-, the green iso-surface represents strong hydrogen bonding between I and –NH–/–NH_2–. Reproduced with permission from ref. 22. Copyright 2014, Royal Society of Chemistry. (b) Structure of MIL-53 (Al) with I_2 adsorbed *via* hydrogen bonding with the hydroxyl groups. Reproduced with permission from ref. 86. Copyright 2017, American Chemical Society. (c) Schematic of triple-helical chains of iodine molecules formed within the channel of MOF MFM-300 (Sc) because of the strong inter-molecular interaction. Reproduced with permission from ref. 88. Copyright 2017, American Chemical Society.

can dissociate to I_2 and I^-, resulting in the release of I_2.[85] Lu *et al.* fabricated a melamine-based polymer (MFP) to stabilize the formed I_3^- species.[23] They claimed that the MFP could effectively capture I_3^- *via* multiple synergistic NH···I hydrogen bonds, and the binding energy was approximately four times higher than that of the conventional Ag–I ionic bond (Fig. 7a). Hydrogen bonding can occur between the proton and the electronegative end of molecular I_2. Paul *et al.* analyzed the potential of three MOFs (MIL-53(Al), MIL-120(Al), and HKUST-1(Cu)) for I_2 adsorption using periodic dispersion density functional theory. They reported that MIL-53 has stronger interactions with I_2 than the other two MOFs.[86] The infrared spectrum simulated *via* molecular dynamics calculations confirmed that this strong interaction originated from the hydrogen bonding between I_2 and the hydroxyl groups of MIL-53 (Fig. 7b).

2.7 Van der Waals interactions

The van der Waals force is a relatively weak but major interaction force. As a nonpolar molecule, I_2 does not have a permanent dipole. However, when close to a charged adsorbent framework, I_2 can interact with the framework by inducing a transient dipole. Accordingly, Shetty *et al.* prepared porous polymers (covalent polycalix[4]arenes) and modified them by lithiation.[87] Compared to the original polymers, lithiated polymers demonstrated faster adsorption kinetics and higher I_2 uptake because of the charge-induced dipole interaction between Li^+ and I_2. In addition to ion-induced dipole interactions, the London dispersion force plays an important role in I_2 capture. For I_2 molecules, temporary dipoles can induce strong intermolecular interactions (dispersion forces), which are influenced by the size and shape of micropores in the adsorbent. For example, the suitable pore geometry MOF MFM-300(Sc) facilitates the self-aggregation of I_2 molecules into an unusual triple helical chain through intermolecular interactions, thus resulting in the efficient packing of I_2 with an exceptional storage density of 3.08 g cm^{-3} (Fig. 7c).[88]

2.8 Hydrophobic interactions

The real off-gas contains a significant amount of moisture, in addition to I_2 and organic iodides. The presence of water molecules poses a significant challenge to I_2 capture because the competitive adsorption of water can significantly reduce the I_2 adsorption capacity. Many strategies used to promote I_2 adsorption, such as Lewis acid–base interactions, Coulomb interactions, and hydrogen bonding, can promote water adsorption. Therefore, adsorption sites capable of preferentially adsorbing I_2 over water are required. Hydrophobic porous materials can selectively capture I_2 in the presence of water *via* hydrophobic interactions because I_2 is a nonpolar hydrophobic molecule. However, such experiments are usually performed at low temperatures[33,89] because relatively weak hydrophobic interactions cannot prevent I_2 desorption at high temperatures.

A chiral polymer zinc D-saccharate having two types of parallel channels, one hydrophilic and the other hydrophobic, has been investigated for I_2 capture.[89] Upon exposure to I_2 vapor, water molecules in the hydrophobic channels are replaced with I_2, while water molecules in the hydrophilic channels remain. This result shows that the preferential adsorption of I_2 over water can be achieved by forming a hydrophobic environment in the adsorbent. Pham *et al.* synthesized a hydrophobicity-intensified silicalite-1 (HISL) zeolite and evaluated its I_2 adsorption properties under various conditions relevant to practical off-gas treatment applications.[33] HISL has similar I_2 adsorption capacity in the presence and absence of water because of its super-hydrophobicity and demonstrates good tolerance to the presence of acids.[33]

3. Mechanisms for methyl iodide capture

In the off-gas from nuclear power plants, CH_3I is produced from a reaction of I_2 with volatile organic compounds (*e.g.*, methane). Compared to I_2, CH_3I is more difficult to capture because of its considerably lower concentration and lack of intermolecular interactions.[90,91] There are relatively few studies on CH_3I capture, and the adsorption strategies employed can be classified broadly into catalytic decomposition reactions, coordination interactions, methylation reactions, halogen bonding, and hydrogen bonding.

3.1 Catalytic decomposition reactions

As in the case of I_2 adsorption, Ag-containing adsorbents, such as Ag-zeolites, can capture CH_3I *via* chemical reactions. For example, Ag^0-MOR zeolite was reported to catalyze the decomposition of CH_3I, where the Brønsted acid sites of the zeolite act as catalytic centers. The surface methoxy species react with other components in the off-gas (*e.g.*, H_2O and NO_x) to form

Open Access Article. Published on 24 2023. Downloaded on 23.04.26 04:24:07.
This article is licensed under a Creative Commons Attribution-NonCommercial 3.0 Unported Licence.

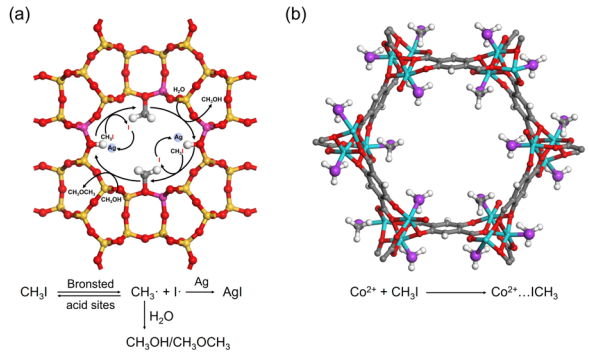

Fig. 8 (a) Schematic of the mechanism of CH_3I adsorption on the Ag^0-MOR zeolite. Brønsted acid sites catalyze the decomposition of CH_3I, and the formed I· reacts with Ag^0 to form AgI, while the CH_3· reacts with H_2O to form by-products such as CH_3OH or CH_3OCH_3. Color code: yellow, Si; red, O; pink, Al; gray, C; and white, H. (b) Crystal structures of CH_3I@Co_2(*p*-DOBDC), where CH_3I reacts with open Co sites by coordination interaction. Reproduced with permission from ref. 95. Copyright 2020, Wiley. Color code: cyan, Co; red, O; purple, I; gray, C; and white, H.

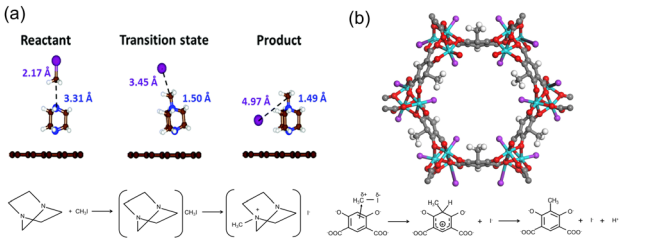

Fig. 9 (a) Calculated geometries of the reactant, transition state, and product during the CH_3I dissociation on the TEDA-modified activated carbon surface. TEDA lowers the dissociation energy of CH_3I and forms quaternary ammonium salt with CH_3I by *N*-methylation reaction. Reproduced with permission from ref. 96. Copyright 1999, Royal Society of Chemistry. (b) Crystal structures of CH_3I@Co_2(*m*-DOBDC) and the proposed mechanism for the reaction between *m*-$DOBDC^{4-}$ and CH_3I. CH_3I reacts with electron-rich *m*-$DOBDC^{4-}$ groups *via* electrophilic aromatic substitution reaction, while the dissociated I^- ions coordinate to the open Co^{2+} sites. Reproduced with permission from ref. 95. Copyright 2020, Wiley. Color code: green, Co; red, O; purple, I; gray, C; and white, H.

volatile by-products. The liberated iodine reacts with Ag in the micropore to form sub-nm AgI clusters (Fig. 8a).[92]

Multiple exchangeable metal cations, including Cu^{2+}, Ag^+, Pb^{2+}, and Na^+, have been introduced into FAU-type X and Y zeolites for CH_3I adsorption.[93] The adsorption capacity of these metal ions followed the order: $Cu^{2+} > Ag^+ \gg Pb^{2+} > Na^+$. This suggests that Cu^{2+} has the highest CH_3I capture efficiency. However, Ag–Y zeolite rather than Cu–Y zeolite was considered the best candidate for CH_3I adsorption because the adsorption of CH_3I on Cu^{2+} leads to undesirable I_2 generation because of the following reaction:

$$Cu^{2+} + 2I^- \rightarrow CuI_2 \rightarrow 2CuI + 1/2I_2 \quad (7)$$

3.2 Coordination interactions

The open metal sites in MOFs can adsorb CH_3I *via* coordination interactions. For example, a mesoporous bimetallic organic framework ECUT-300-200-Ac was synthesized with purposely generated structural defects that render many open metal sites.[94] XPS revealed a blue shift of the Cd_{3d} and U_{4f} binding energies in ECUT-300-200-Ac when exposed to CH_3I, indicating the participation of these metal sites in adsorption. Similarly, SXRD indicated that MOF Co_2(*p*-DOBDC) can adsorb CH_3I at its open Co sites through coordination, with the I end of the CH_3I molecule interacting with Co in a side-on configuration (Fig. 8b).[95]

3.3 Methylation reactions

Another effective strategy to capture CH_3I is to functionalize the adsorbent with multiple amine groups that can bind CH_3I *via* *N*-methylation reactions. For example, a number of nucleophilic amines, including triethylenediamine (TEDA), hexamethylenetetramine (HMTA), *N*,*N*′-dimethylethylenediamine, *N*,*N*′-dimethyl-1,3-propanediamine, and *N*,*N*′-dimethyl-1,4-butanediamine, were loaded onto activated carbon by impregnation to enhance their CH_3I binding strength.[12] Density functional theory (DFT) calculations and *ab initio* molecular dynamics simulations indicate that TEDA can reduce the dissociation activation barrier of CH_3I and participate in the subsequent alkylation to form a quaternary ammonium salt (Fig. 9a).[96] For example, tertiary amines, TEDA and HMTA, were grafted to the open metal sites of MIL-101 (Cr) for CH_3I capture. The resulting MIL-101-Cr-TED exhibited an ultrahigh CH_3I uptake of 71 wt% at 150 °C, which is more than three times that of Ag^0-MOR.[97] In addition to tertiary aliphatic amines, aromatic N species have been used to capture CH_3I through *N*-methylation reactions, such as pyridine-*N*,[98] aniline-*N*,[25] pyrazole-*N*,[94] imine-*N*, and triazine-*N*.[99]

The adsorbent can also capture CH_3I through electrophilic aromatic substitution reactions. Park *et al.* synthesized two MOFs, Co_2(*m*-DOBDC) and Co_2(*p*-DOBDC), and compared their structures after CH_3I adsorption.[95] SXRD indicated that CH_3I reacted with electron-rich *m*-$DOBDC^{4-}$ groups, converting the aryl C–H bond to the C–C bond, with the dissociated I^- coordinating to the open Co^{2+} sites (Fig. 9b). However, for the isostructural Co_2(*p*-DOBDC) lacking electron-rich C, CH_3I was coordinately adsorbed at the open Co^{2+} sites without undergoing electrophilic aromatic substitution (Fig. 8b).

3.4 Halogen bonding and hydrogen bonding

Quantum chemical calculations report that halogen bonds may play an important role in promoting CH_3I adsorption when electron-rich moieties are present in the adsorbent. For example, CH_3I can form weak halogen bonds with –C=N– in 1,2-dihydrophenazine in polymer MHP-P5Q, in which the bond length $d_{[N\cdots I]}$ is 3.39 Å (Fig. 10a).[25] A halogen bond between I and an electron-rich group appears counterintuitive because halogen atoms are electronegative. Brinck *et al.* theoretically explained this.[100] They reported that the electrostatic potential of covalently bonded halogens is anisotropic and possesses

 This journal is © The Royal Society of Chemistry 2023

Open Access Article. Published on 24 2023. Downloaded on 23.04.26 04:24:07.
This article is licensed under a Creative Commons Attribution-NonCommercial 3.0 Unported Licence.

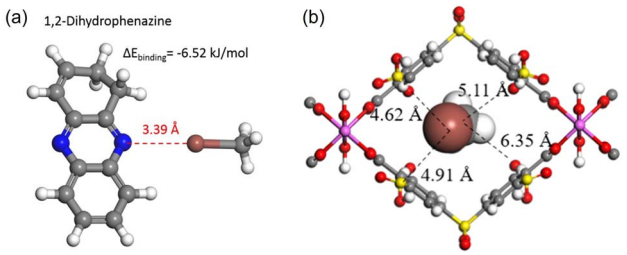

Fig. 10 (a) Calculated structure of CH_3I interacting with 1,2-dihydrophenazine, showing that CH_3I forms weak halogen bonds with –C═N– in a head-on configuration. Reprinted with permission from ref. 25. Copyright 2020, Springer Nature. Color code: gray, C; white, H; blue, N; brown, I. (b) DFT-optimized structure of CH_3I in the CAU-11-SO_3H pore channel, showing that CH_3I interacts with the modified sulfonic acid by I···O and I···S electrostatic interactions. Color code: gray, C; white, H; red, O; pink, Al; brown, I and yellow, S. Reprinted with permission from ref. 101. Copyright 2021, American Chemical Society.

positive regions at the tip of X (X = Cl, Br, and I). Therefore, halogen bonds can be formed between CH_3I with nucleophiles in a head-on configuration.

In a purely theoretical study, Wu *et al.* screened a series of Al-based MOFs for CH_3I capture from the simulated off-gas using Grand canonical Monte Carlo (GCMC) simulations and DFT calculations.[101] Among the MOFs evaluated, CAU-11 with 1D narrow channels demonstrated the highest isosteric heat (Q_{st}) of CH_3I. Note that additional modification of CAU-11 with sulfonic acid groups enabled highly efficient capture of trace CH_3I, which was attributed to the formation of I···O and I···S electrostatic interactions (Fig. 10b). Such interactions were not assigned as halogen bonds possibly because the calculated configuration of CH_3I was "side-on" rather than "head-on".

Endowing adsorbents with hydrogen bonding sites is another approach for promoting their CH_3I capture capability. Unlike halogen bonding, when CH_3I is immobilized by hydrogen bonding, the iodine atom acts as an electron donor.[102] Chebbi *et al.* compared the CH_3I capture capability of a number of MOFs, including ZIF-8 (Zn), MIL-53 (Al), MIL-100 (Al), UiO-66 (Zr), HKUST-1 (Cu), CAU-1 (Al), and MIL-120 (Al). They reported that MIL-120 (Al) had the strongest interaction with CH_3I because of its abundant –OH groups, which promoted the formation of H-bonded complexes with CH_3I.[103] The captured CH_3I could not be desorbed from MIL-120 (Al) by He evacuation.

4. Performance evaluation

The adsorbents developed for I_2/CH_3I capture can be evaluated under static or dynamic conditions or both. Static measurements are easy to operate but have multiple limitations. Whereas dynamic measurements require the development of gas circuits and the use of detectors, they provide more flexible test conditions relevant to practical applications. This section describes typically used static and dynamic systems and their applications for I_2 and CH_3I adsorption measurements.

4.1 Static measurement

In most studies on I_2 (or CH_3I) capture, the adsorption capacity of the adsorbent is measured under static conditions using a closed system, in which I_2 (or CH_3I) and the adsorbent are heated simultaneously to the target temperature (Fig. 11a). After some time (assuming adsorption equilibrium has been achieved), the system is cooled to room temperature, and the adsorption capacity is determined based on the mass increase of the adsorbent. The static system is also used to determine the adsorption kinetics by recording the mass changes at different time intervals. The commonly used index for adsorption kinetics is $K_{80\%}$, which refers to the average adsorption rate before the adsorption capacity reaches 80%.[104]

Despite its simplicity and widespread use, there are several problems with such a static measurement system. For example, static I_2 adsorption is typically conducted at 75 °C and ambient pressure; under such conditions, the partial pressure of I_2 is 1.6 kPa. The corresponding I_2 volumetric concentration is $\sim 1.6 \times 10^4$ ppmv, which is several orders of magnitude higher than the actual I_2 concentration in the off-gas. Hence, the measured I_2 adsorption capacity does not truly reflect the I_2 capture performance in practical applications. Moreover, during the cooling process of the system, a large amount of I_2 may condense on the surface of the adsorbent and the vial containing the adsorbent, resulting in a considerable overestimation of the adsorption capacity. Although using an empty vial as a blank control can eliminate this overestimation to a certain extent (Fig. 11a), the adsorption capacity determined in this manner remains

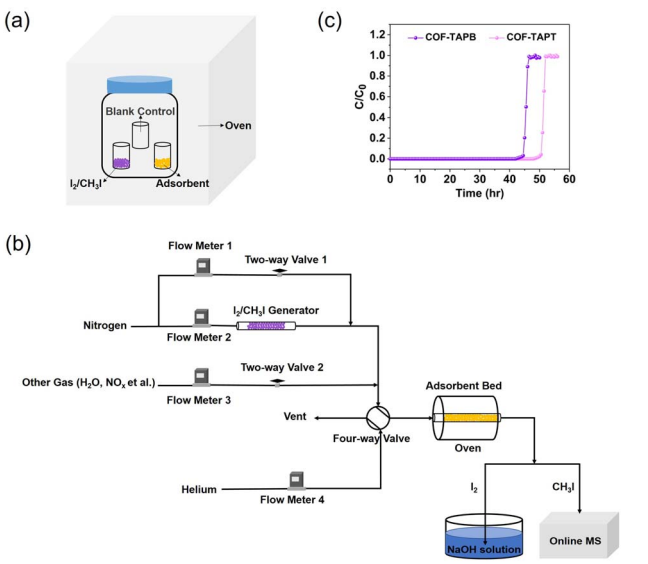

Fig. 11 (a) Schematic of the static system used to measure the I_2 or CH_3I adsorption capacity of adsorbents. (b) Schematic of the dynamic system used to measure the I_2 or CH_3I adsorption capacity of adsorbents, which is based on a column breakthrough setup. The concentration of I_2 in the effluent can be determined by collecting I_2 using NaOH solution followed by elemental analysis using ICP-MS. (c) Typical breakthrough profiles obtained from the dynamic measurement to determine the adsorption capacity. Reproduced with permission from ref. 99. Copyright 2022, Springer Nature.

Open Access Article. Published on 24 2023. Downloaded on 23.04.26 04:24:07.
This article is licensed under a Creative Commons Attribution-NonCommercial 3.0 Unported Licence.

unreliable. This can explain why certain reported adsorption capacities are considerably higher than the theoretical values calculated based on the adsorbent pore volume.[105–109] Moreover, using a static measurement system, it is impossible to control the I_2 concentration and adsorption temperature independently or co-feed other components, such as H_2O and NO_x, to simulate the actual off-gas conditions.

Considering these limitations and problems, using such a static measurement system to evaluate the performance of adsorbents for I_2 capture is not recommended. Compared to I_2, CH_3I has weaker intermolecular forces and is less prone to condensation. Therefore, the CH_3I adsorption capacity determined using a static system is relatively more reliable. However, when CH_3I is adsorbed *via* chemical reactions (for example, when CH_3I is adsorbed on Ag-zeolites), the adsorption capacity cannot be determined accurately by the mass change because of the production of volatile byproducts such as CH_3OH and CH_3OCH_3.

Compared to the I_2 capture, which has been extensively studied, there are only a few studies of CH_3I capture. Xie *et al.* compared the different adsorption behavior of CH_3I and I_2 under static and dynamic conditions using specially designed COFs as adsorbents.[99] They reported that I_2 adsorption is dominated by intermolecular interactions under commonly used static evaluation conditions (saturated I_2 vapor at 75 °C). The capacity is primarily determined by the textural properties (surface area and pore volume) of the adsorbent. However, the CH_3I adsorption capacity depends on the number of strong binding sites of the adsorbent rather than its textural properties, thus exhibiting a positive correlation with the N content (strong binding sites) in the COFs. The observed one-to-one correspondence between CH_3I and N suggests that CH_3I molecules are only adsorbed on N sites possibly by forming salts.[99] The adsorption kinetics of I_2 and CH_3I on these COFs demonstrate a similar trend, *i.e.*, they are primarily determined by the textural properties and the number of strong binding sites, respectively.

4.2 Dynamic measurement

The problems associated with the static system can be circumvented by dynamic adsorption measurements using a fixed-bed setup (Fig. 11b). The dynamic measurement system allows free adjustment of the I_2/CH_3I concentration, precise control of the adsorbent temperature, and easy simulation of off-gas compositions.[110] Importantly, it is close to the actual application scenario using adsorbent-packed columns to capture iodine.

In a dynamic system, the carrier gas flows continuously through the I_2/CH_3I generator to produce I_2/CH_3I vapor, the concentration of which can be adjusted by the dilution gas. The adsorbent is separated from the vapor generator, and its temperature can be controlled independently using an oven. Other substances can be introduced into the system with independent gas lines to simulate the off-gas composition (Fig. 11b). Breakthrough curves can be plotted by analyzing the I_2/CH_3I content in the outlet gas *via* inductively coupled plasma mass spectrometry (ICP-MS) and online mass spectrometry, respectively (Fig. 11c). From this, a reliable adsorption capacity can be determined by curve integration (eqn (8)):

$$q = \frac{F_i \times t_0 - V_{dead} - \int_0^{t_0} F_e \Delta t}{m} \quad (8)$$

where F_i is the influent flow rate of the I_2/CH_3I (mL min^{-1}); t_0 is the adsorption time (min); V_{dead} is the dead volume of the system (cm^3); F_e is the effluent flow rate of I_2/CH_3I (mL min^{-1}); and m is the weight of the adsorbents (g).

Han *et al.* used a dynamic system to measure the I_2 uptake capacity of an ionic COF (iCOF-AB-50) at a low I_2 concentration of 400 ppmv and 25 °C.[111] They attributed the high I_2 uptake capacity (2.79 g g^{-1}) to the combination of high pore volume and abundant binding sites in iCOF-AB-50. Moreover, they examined the effects of competitive water adsorption on the I_2 capture of iCOF-AB-50 by introducing water vapor (relative humidity: 50%) to the dynamic I_2 adsorption system at 25 °C. The presence of water vapor caused only a slight decrease in the I_2 uptake of iCOF-AB-50 to 2.70 g g^{-1} compared to that without water vapor addition (2.79 g g^{-1}), during which a certain amount of water was adsorbed. This suggests that although iCOF-AB-50 is not completely water-repellant, most of its adsorptive sites bind preferentially to I_2, thus leaving their I_2 adsorption capacity almost intact under humid conditions.

In a more recent study, the same group developed a guanidinium-based ionic COF, termed TGDM, and evaluated its I_2 capture ability using a dynamic measurement system.[84] The tests were conducted at 150 ppmv of I_2 and 150 °C to simulate the actual off-gas conditions. Under low-concentration and high-temperature conditions, TGDM exhibited significantly higher I_2 uptake capacity than iCOF-AB-50 (0.3 *vs.* 0.08 g g^{-1}) despite its lower pore volume. Compared with iCOF-AB-50, the superior high-temperature I_2 capture performance of TGDM was attributed to its higher density of ionic groups and improved thermal stability.

The CH_3I concentration in the off-gas of actual nuclear power plants is extremely low, typically <50 ppmv. However, most studies on CH_3I capture evaluated the adsorbents at considerably higher CH_3I concentrations (*e.g.*, 2×10^5 ppmv), even with a dynamic system.[94,97,98] Among the adsorbents investigated, mesoporous MOF ECUT-300-200-Ac demonstrated record CH_3I uptake capacities of > 2.8 g g^{-1} at 25 °C and > 0.87 g g^{-1} at 150 °C. Its excellent CH_3I capture ability was attributed to the combined effects of coordination interactions, methylation reactions, and hydrogen bonding.[94] Han *et al.* compared the CH_3I capture performance of multiple state-of-the-art adsorbents at 50 ppmv of CH_3I and 25 °C.[99] The CH_3I adsorption capacities obtained were as follows: MIL-101-Cr-HMTA[97] (0.51 g g^{-1}) > COF-TAPT[99] (0.39 g g^{-1}) > TFPA-TAPT[99] (0.18 g g^{-1}) > COF-TAPB[99] ≈ iCOF-AB-50 [111] (0.12 g g^{-1}) > SCU-COF-2 [98] (0.08 g g^{-1}). These results confirm that the adsorption of CH_3I is determined primarily by the type and number of binding sites and is not related significantly to the textural properties of the adsorbent. These results indicate that unlike I_2 adsorption, ionic groups have little effect on CH_3I adsorption, which may be because I_2 readily forms charged polyiodide species, such as I_3^- and I_5^-, whereas CH_3I cannot.

 This journal is © The Royal Society of Chemistry 2023

Open Access Article. Published on 24 2023. Downloaded on 23.04.26 04:24:07.
This article is licensed under a Creative Commons Attribution-NonCommercial 3.0 Unported Licence.

Table 1 I_2/CH_3I capture performance of various adsorbents tested using dynamic systems

		Adsorbent name	Test temperature (°C)	Vapor concentration (ppmv)	Adsorption capacity (g g^{-1})	Adsorption mechanisms	Ref.
I_2 capture	Inorganic materials	Ag^0Z	150	50	0.12	Redox reaction	112
		HISL	RT	400	0.53	Hydrophobic interaction	33
		SL-1	RT	400	0.48	Hydrophobic interaction	33
		Si-BEA	RT	400	0.47	Hydrophobic interaction	33
		AC	RT	400	0.70	Van der Waals interaction	33
		23Ag/Y	100	1250	0.22	Redox reaction	113
		35Ag/13X	100	1250	0.46	Redox reaction	113
		C@ETS-10	20	32	0.04	Van der Waals interaction	114
	MOFs	HKUST-1	RT	400	0.38	Hydrogen bonding	33
		ZIF-8	RT	400	0.03	Lewis acid–base interaction	33
		MIL-101-Cr-HMTA	25	150	0.83	Lewis acid–base interaction	99
	COFs	iCOF-AB-50	25	400	2.79	Coulomb interaction	111
		iCOF-AB-50	25	150	1.52	Coulomb interaction	99
		iCOF-AB-50	75	400	0.44	Coulomb interaction	111
		SCU-COF-2	25	400	0.98	Lewis acid–base interaction	98
		SCU-COF-2	25	150	0.49	Lewis acid–base interaction	99
		SCU-COF-2	75	400	0.35	Lewis acid–base interaction	98
		TGDM	150	150	0.30	Coulomb interaction	84
		JUC-561	150	150	0.20	Lewis acid–base interaction	84
		COF-TAPT	25	150	1.25	Lewis acid–base interaction	99
		COF-TAPB	25	150	1.12	Lewis acid–base interaction	99
		TFPA-TAPT	25	150	0.42	Lewis acid–base interaction	99
	POPs	POSS-TPPSe	160	0.16	0.26	Lewis acid–base interaction	78
CH_3I capture	Inorganic materials	22.8Ag/Y	35	1333	0.25	Catalytic decomposition reaction	115
		22.8Ag/Y	100	1333	0.223	Catalytic decomposition reaction	115
		22.8Ag/Y	250	1333	0.193	Catalytic decomposition reaction	115
		Ag^+@13X	150	200 000	0.48	Catalytic decomposition reaction	97
		TED@AC	150	200 000	0.17	Methylation reaction	97
		HMTA@AC	150	200 000	0.14	Methylation reaction	97
		Ag^+@ZSM-5	150	200 000	0.24	Catalytic decomposition reaction	97
		HISL	25	532 967	0.42	—	33
	MOFs	MIL-101-Cr-TED	30	200 000	1.60	Methylation reaction	97
		MIL-101-Cr-TED	150	200 000	0.71	Methylation reaction	97
		MIL-101-Cr-HMTA	30	200 000	1.74	Methylation reaction	97
		MIL-101-Cr-HMTA	150	200 000	0.62	Methylation reaction	97
		MIL-101-Cr-HMTA	25	50	0.51	Methylation reaction	99
		ECUT-300-200-Ac	25	200 000	2.80	Methylation reaction/hydrogen bonding/ coordination interaction	94
		ECUT-300-200-Ac	150	200 000	0.87	Methylation reaction/hydrogen bonding/ coordination interaction	94
		MIL-53	35	1333	0.13	Hydrogen bonding	103
		MIL-120	35	1333	0.16	Hydrogen bonding	103
		HKUST-1	35	1333	0.43	Coordination interaction	103
		MIL-101-RSO_3Ag	30	20	0.16	Coordination interaction	116

Open Access Article. Published on 24 2023. Downloaded on 23.04.26 04:24:07.
This article is licensed under a Creative Commons Attribution-NonCommercial 3.0 Unported Licence.

Table 1 (*Contd.*)

	Adsorbent name	Test temperature (°C)	Vapor concentration (ppmv)	Adsorption capacity (g g^{-1})	Adsorption mechanisms	Ref.
COFs	SCU-COF-2	25	200 000	0.564	Methylation reaction	98
	SCU-COF-2	75	200 000	0.17	Methylation reaction	98
	SCU-COF-2	25	50	0.08	Methylation reaction	99
	iCOF-AB-50	25	200 000	0.62	—	99
	iCOF-AB-50	25	50	0.11	—	99
	COF-TAPT	25	200 000	1.30	Methylation reaction	99
	COF-TAPT	25	50	0.39	Methylation reaction	99
	COF-TAPB	25	200 000	0.71	Methylation reaction	99
	COF-TAPB	25	50	0.12	Methylation reaction	99
	TFPA-TAPT	25	50	0.18	Methylation reaction	99

Few studies have used dynamic systems to test the I_2/CH_3I capture performance of adsorbents. Table 1 lists the relevant results reported in the literature.

5. Simultaneous capture of low-concentration I_2 and CH_3I

Molecular iodine and organic iodides (represented by CH_3I) coexist in the off-gas of nuclear power plants at low concentrations, and both need to be captured. Because of their different properties, it is important to develop adsorbents that can capture both I_2 and CH_3I with high efficiency. However, few studies have evaluated the ability of adsorbents to simultaneously capture I_2 and CH_3I (Table 2), possibly because such measurements require dynamic adsorption systems that are difficult to operate and are less common.

Li *et al.* modified MOF MIL-101 (Cr) with various tertiary amines to simultaneously capture I_2 and CH_3I under simulated off-gas conditions.[97] The tertiary amine groups can adsorb I_2 through Lewis acid–base interactions and adsorb CH_3I through methylation reactions. Consequently, amine-functionalized MIL-101 (Cr) MOFs exhibit high total iodine (I_2 + CH_3I) uptake when used for iodine capture from gas streams containing 150 ppmv I_2 and 50 ppmv CH_3I in the presence of HNO_3, NO_x, and water vapor. Specific iodine uptake depends on the density of the amine groups and test temperature (Table 2). At 150 °C, both MIL-101-Cr-TED and MIL-101-Cr-HMDA rendered a "decontamination factor" (DF) value as high as > 5000, which met the regulatory standards of nuclear processing facilities (DF > 3000).

Xie *et al.* reported the iodine capture performance of several COFs from gas streams containing 150 ppmv I_2 and 50 ppmv CH_3I at 25 °C.[99] Two COF materials (iCOF-AB-50 and COF-TAPT) ranked the top two among all the adsorbents evaluated, with a total iodine uptake of 1.59 and 1.51 g g^{-1}, respectively. These values are higher than the total iodine uptake of MIL-101-Cr-HMDA (1.08 g g^{-1}) obtained under the same conditions. According to the single-component dynamic adsorption results, the ultrahigh total iodine uptake of iCOF-AB-50 is derived from the contribution of I_2 adsorption because of the abundant ionic groups that effectively promote I_2 adsorption *via* strong Coulomb interactions.

6. Summary and outlook

Over the past decade, many nanoporous materials, primarily COFs, POPs, and MOFs, have been reported as adsorbents for iodine capture. Compared to traditional industrial adsorbents, such as zeolites and activated carbon, these emerging adsorbents are characterized by easily regulated pore structures and abundant surface functionality, enabling the capture of molecular iodine and organic iodides *via* novel adsorption mechanisms.

This review summarizes the common mechanisms for adsorption-based iodine capture. Molecular iodine can be adsorbed *via* redox reactions, coordination interactions,

This journal is © The Royal Society of Chemistry 2023

Open Access Article. Published on 24 2023. Downloaded on 23.04.26 04:24:07.
This article is licensed under a Creative Commons Attribution-NonCommercial 3.0 Unported Licence.

Table 2 Summary of the reported results for the simultaneous capture of I_2 and CH_3I

	Adsorbent name	Test temperature (°C)	I_2 concentration (ppmv)	CH_3I concentration (ppmv)	Total iodine uptake (g g^{-1})	Adsorption mechanisms	Ref.
Zeolites	Ag^0@MOR	150	150	50	0.16[a]	Redox reaction/catalytic decomposition reaction	97
	Ag^0@MOR	25	150	50	0.44[a]	Redox reaction/catalytic decomposition reaction	97
	HISL	150	150	50	0.05[a]	Hydrophobic interaction	97
	HISL	25	150	50	0.08[a]	Hydrophobic interaction	97
MOFs	MIL-101-Cr-TED	25	150	50	0.55[a]	Lewis acid–base interaction/methylation reaction	97
	MIL-101-Cr-TED	150	150	50	0.38[a]	Lewis acid–base interaction/methylation reaction	97
	MIL-101-Cr-HMTA	25	150	50	0.44[a]	Lewis acid–base interaction/methylation reaction	97
	MIL-101-Cr-HMTA	150	150	50	0.33[a]	Lewis acid–base interaction/methylation reaction	97
	MIL-101-Cr-HMTA	25	150	50	1.08[b]	Lewis acid–base interaction/methylation reaction	99
COFs	SCU-COF-2	25	150	50	0.56[b]	Lewis acid–base interaction/methylation reaction	99
	iCOF-AB-50	25	150	50	1.59[b]	Coulomb interaction	99
	COF-TAPT	25	150	50	1.51[b]	Lewis acid–base interaction/methylation reaction	99
	COF-TAPB	25	150	50	1.17[b]	Lewis acid–base interaction/methylation reaction	99
	TFPA-TAPT	25	150	50	0.47[b]	Lewis acid–base interaction/methylation reaction	99

[a] The experiment was conducted under the conditions of simulated gas mixtures, including I_2 (150 ppmv), CH_3I (50 ppmv), humidity (RH = 95%), HNO_3, and NO_x. [b] The experiment was conducted with the mixed vapor of 150 ppm I_2 and 50 ppm CH_3I.

Open Access Article. Published on 24 2023. Downloaded on 23.04.26 04:24:07.
This article is licensed under a Creative Commons Attribution-NonCommercial 3.0 Unported Licence.

electrophilic aromatic substitution, Lewis acid–base interactions, Coulomb interactions, hydrogen bonding, van der Waals interactions, and hydrophobic interactions. As a representative of organic iodides, CH_3I can be adsorbed *via* catalytic decomposition reactions, coordination interactions, methylation reactions, halogen bonding, and hydrogen bonding. In general, CH_3I is extremely difficult to capture by physisorption than I_2 because of the lack of strong intermolecular forces and its ultra-low concentration in the off-gas.

Despite the multiple studies on iodine capture in recent years, most did not consider the needs of practical applications. The adsorbents for capturing iodine from actual off-gas require to meet two requirements because the off-gas produced during the reprocessing of used fuel rods generally has high temperatures (~150 °C), low concentrations of I_2 (<150 ppmv) and organic iodides (~50 ppmv), and various acidic (pH < 1) components and water vapor. First, they should be able to capture iodine at low concentrations and high temperatures. Second, they should be chemically and thermally stable under strongly acidic hydrothermal conditions.

However, previous studies did not consider these two important factors when examining whether the adsorbent has practical value. Indeed, a vast majority of "emerging" adsorbents, such as MOFs, COFs, and POPs, were evaluated at low temperatures (≤75 °C) with high I_2 concentrations (using saturated I_2 vapor). As high temperature and low I_2 concentration are unfavorable factors for I_2 adsorption, the I_2 uptake of these adsorbents under the actual industrial conditions must be considerably lower than the reported values. Therefore, the reported adsorption capacity is meaningless for practical applications, and the static measurement method is unreliable (Section 4.1). Another neglected issue is the stability of the adsorbents under the hydrothermally acidic conditions of industrial off-gas. The intrinsic porous structures of organic or organic–inorganic hybrid adsorbents can be destroyed under harsh conditions with few exceptions.[84,97,99] Structural damage to adsorbents indicates a significant reduction in adsorption capacity and loss of reusability.

Based on these considerations, although organic-based adsorbents are valuable for fundamental research, they are unlikely to be directly applied to capture iodine from industrial off-gas. They may be useful for capturing iodine from pretreated off-gas to remove moisture and reduce acidity at lower temperatures or under other mild-condition applications. It remains a considerable challenge to develop high-performance adsorbents for direct off-gas treatment that combine high iodine uptake with excellent structural stability and reusability. Considering the highly unfavorable adsorption conditions (*i.e.*, high temperature of ~150 °C and low iodine concentration), the desired iodine adsorption capacity is difficult to achieve by physisorption, whereas chemisorption may be the only option because of its high adsorption strength. Therefore, the ideal adsorbents for iodine capture from off-gas should have many easily regenerated chemisorption sites while maintaining structural integrity during adsorption and regeneration. Achieving this goal may require new adsorption strategies. For example, a single strong binding site can make regeneration difficult, but coupling several moderately strong binding sites may provide a balance between adsorption efficiency and recyclability. To avoid structural damage, it is necessary to understand the mechanisms responsible for the structural degradation of adsorbents caused by common species in nuclear off-gas. In this regard, quantum chemistry calculations and simulations would be a useful tool. The revealed adsorbate–adsorbent interaction modes can provide insight into the degradation mechanism, thereby guiding the design of stable iodine adsorbents.

Dynamic measurement systems are recommended for evaluating developed adsorbents because they can easily realize precise concentration and temperature control while allowing the incorporation of multiple components to simulate the actual application conditions and scenarios. For example, the experiments of simultaneously capturing I_2 and CH_3I can be easily performed using a dynamic system. Competitive adsorption between I_2/CH_3I and coexisting species in the off-gas, including H_2O, NO, CO, CH_3Cl, and Cl_2, can be investigated using a dynamic system. There is still a lack of systematic research on the competitive adsorption of these components, except for a few studies focusing only on water. Finally, this study proposes to evaluate the adsorbents developed for iodine capture under conditions close to actual off-gas. Alternatively, researchers should discuss the correlation between the test conditions and specific application scenarios.

Conflicts of interest

There are no conflicts to declare.

Acknowledgements

This research is supported by the AMPM CCF fund (FCC/1/1972-43-01) to Y. H. from King Abdullah University of Science and Technology.

Notes and references

1 I. A. E. Agency, **https://www.iaea.org/newscenter/news/the-use-of-nuclear-power-beyond-generating-electricity-non-electric-applications**.
2 E. Kintisch, *Science*, 2005, **310**, 1406.
3 J. E. Ten Hoeve and M. Z. Jacobson, *Energy Environ. Sci.*, 2012, **5**, 8743–8757.
4 P. A. Kharecha and J. E. Hansen, *Environ. Sci. Technol.*, 2013, **47**, 4889–4895.
5 F. C. Kupper, M. C. Feiters, B. Olofsson, T. Kaiho, S. Yanagida, M. B. Zimmermann, L. J. Carpenter, G. W. Luther, Z. L. Lu, M. Jonsson and L. Kloo, *Angew. Chem., Int. Ed.*, 2011, **50**, 11598–11620.
6 A. Saiz-Lopez, J. M. C. Plane, A. R. Baker, L. J. Carpenter, R. von Glasow, J. C. G. Martin, G. McFiggans and R. W. Saunders, *Chem. Rev.*, 2012, **112**, 1773–1804.
7 K. Nakamura, M. Saeki and E. Tachikaw, *J. Nucl. Sci. Technol.*, 1973, **10**, 367–373.

 This journal is © The Royal Society of Chemistry 2023

Open Access Article. Published on 24 2023. Downloaded on 23.04.26 04:24:07.
This article is licensed under a Creative Commons Attribution-NonCommercial 3.0 Unported Licence.

8 E. C. Beahm, Y. M. Wang, S. J. Wisbey and W. E. Shockley, *Nucl. Technol.*, 1987, **78**, 34–42.
9 J. Paquette and B. L. Ford, *Abstr. Pap. Am. Chem. Soc.*, 1988, **195**, 88–Nucl.
10 D. R. Haefner and T. J. Tranter, Report No. INL/EXT-07-12299; TRN: US0800243, 2007.
11 S. U. Nandanwar, K. Coldsnow, V. Utgikar, P. Sabharwall and D. E. Aston, *Chem. Eng. J.*, 2016, **306**, 369–381.
12 C. M. Gonzalez-Garcia, J. F. Gonzalez and S. Roman, *Fuel Process. Technol.*, 2011, **92**, 247–252.
13 N. Mnasri, C. Charnay, L. C. de Menorval, Y. Moussaoui, E. Elaloui and J. Zajac, *Microporous Mesoporous Mater.*, 2014, **196**, 305–313.
14 Q. H. Cheng, Z. J. Li and T. W. Chu, *Nucl. Sci. Technol.*, 2015, **26**, 43–47.
15 Y. Nan, L. L. Tavlarides and D. W. DePaoli, *AIChE J.*, 2017, **63**, 1024–1035.
16 H. J. Choi and M. P. Suh, *J. Am. Chem. Soc.*, 2004, **126**, 15844–15851.
17 M. H. Zeng, Q. X. Wang, Y. X. Tan, S. Hu, H. X. Zhao, L. S. Long and M. Kurmoo, *J. Am. Chem. Soc.*, 2010, **132**, 2561–2563.
18 N. X. Zhu, C. W. Zhao, J. C. Wang, Y. A. Li and Y. B. Dong, *Chem. Commun.*, 2016, **52**, 12702–12705.
19 B. Guo, F. Li, C. Wang, L. Zhang and D. Sun, *J. Mater. Chem. A*, 2019, **7**, 13173–13179.
20 T. Xu, J. T. Li, M. W. Jia, G. H. Li and Y. L. Liu, *Dalton Trans.*, 2021, **50**, 13096–13102.
21 G. Das, T. Prakasam, S. Nuryyeva, D. S. Han, A. Abdel-Wahab, J. C. Olsen, K. Polychronopoulou, C. Plataslglesias, F. Ravaux, M. Jouiad and A. Trabolsi, *J. Mater. Chem. A*, 2016, **4**, 15361–15369.
22 T. Geng, Z. Zhu, W. Zhang and Y. Wang, *J. Mater. Chem. A*, 2017, **5**, 7612–7617.
23 J. Wang, Z. L. Li, Y. Wang, C. T. Wei, K. L. Ai and L. H. Lu, *Mater. Horiz.*, 2019, **6**, 1517–1525.
24 W. Xie, D. Cui, S. R. Zhang, Y. H. Xu and D. L. Jiang, *Mater. Horiz.*, 2019, **6**, 1571–1595.
25 K. C. Jie, Y. J. Zhou, Q. Sun, B. Li, R. Zhao, D. E. Jiang, W. Guo, H. Chen, Z. Z. Yang, F. H. Huang and S. Dai, *Nat. Commun.*, 2020, **11**, 1086.
26 M. Y. Xu, T. Wang, L. Zhou and D. B. Hua, *J. Mater. Chem. A*, 2020, **8**, 1966–1974.
27 Y. S. Lan, M. M. Tong, Q. Y. Yang and C. L. Zhong, *Crystengcomm*, 2017, **19**, 4920–4926.
28 J. H. Li, H. X. Zhang, L. Y. Zhang, K. Wang, Z. K. Wang, G. Y. Liu, Y. L. Zhao and Y. F. Zeng, *J. Mater. Chem. A*, 2020, **8**, 9523–9527.
29 L. Y. Zhang, J. H. Li, H. X. Zhang, Y. Liu, Y. M. Cui, F. C. Jin, K. Wang, G. Y. Liu, Y. L. Zhao and Y. F. Zeng, *Chem. Commun.*, 2021, **57**, 5558–5561.
30 P. Wang, Q. Xu, Z. P. Li, W. M. Jiang, Q. H. Jiang and D. L. Jiang, *Adv. Mater.*, 2018, **30**, 1801991.
31 Q. Zhao, L. Zhu, G. Lin, G. Chen, B. Liu, L. Zhang, T. Duan and J. Lei, *ACS Appl. Mater. Interfaces*, 2019, **11**, 42635–42645.
32 T.-M. Geng, F.-Q. Wang, X.-C. Fang and H. Xu, *Microporous Mesoporous Mater.*, 2021, **317**, 111001.
33 T. C. T. Pham, S. Docao, I. C. Hwang, M. K. Song, D. Y. Choi, D. Moon, P. Oleynikov and K. B. Yoon, *Energy Environ. Sci.*, 2016, **9**, 1050–1062.
34 K. W. Chapman, P. J. Chupas and T. M. Nenoff, *J. Am. Chem. Soc.*, 2010, **132**, 8897–8899.
35 Y. Lu, H. W. Liu, R. N. Gao, S. L. Xiao, M. Zhang, Y. F. Yin, S. Q. Wang, J. Li and D. J. Yang, *ACS Appl. Mater. Interfaces*, 2016, **8**, 29179–29185.
36 R. N. Gao, Y. Lu, S. L. Xiao and J. Li, *Sci. Rep.*, 2017, **7**, 4303.
37 D. W. Holladay, Literature survey: methods for the removal of iodine species from off-gases and liquid waste streams of nuclear power and nuclear fuel reprocessing plants, with emphasis on solid sorbents, *Oak Ridge National Lab.*(ORNL), Report No. ORNL/TM-6350, 1979, DOI: **10.2172/6394859**.
38 J. Huve, A. Ryzhikov, H. Nouali, V. Lalia, G. Auge and T. J. Daou, *RSC Adv.*, 2018, **8**, 29248–29273.
39 J. H. Yang, Y. J. Cho, J. M. Shin and M. S. Yim, *J. Nucl. Mater.*, 2015, **465**, 556–564.
40 H. Zou, F. C. Yi, M. X. Song, X. Q. Wang, L. Bian, W. M. Li, N. Pan and X. Q. Jiang, *J. Hazard. Mater.*, 2019, **365**, 81–87.
41 A. T. Reda, M. Pan, D. X. Zhang and X. Y. Xu, *J. Environ. Chem. Eng.*, 2021, **9**, 105279.
42 S. W. Kang, J. H. Yang and M. S. Yim, *Nucl. Technol.*, 2020, **206**, 1593–1606.
43 X. R. Zhang, I. da Silva, R. Fazzi, A. M. Sheveleva, X. Han, B. F. Spencer, S. A. Sapchenko, F. Tuna, E. J. L. McInnes, M. Li, S. H. Yang and M. Schroder, *Inorg. Chem.*, 2019, **58**, 14145–14150.
44 E. Baladi, V. Nobakht, A. Tarassoli, D. M. Proserpio and L. Carlucci, *Cryst. Growth Des.*, 2018, **18**, 7207–7218.
45 B. Lee, Y. P. Chen, J. Park and J. Park, *ACS Appl. Mater. Interfaces*, 2019, **11**, 25817–25823.
46 A. Y. Rogachev and R. Hoffmann, *J. Am. Chem. Soc.*, 2013, **135**, 3262–3275.
47 D. F. Sava, K. W. Chapman, M. A. Rodriguez, J. A. Greathouse, P. S. Crozier, H. Y. Zhao, P. J. Chupas and T. M. Nenoff, *Chem. Mater.*, 2013, **25**, 2591–2596.
48 J. H. Ye, Z. J. Hu, Y. X. Wang, W. C. Zhang and Y. Zhang, *Tetrahedron Lett.*, 2012, **53**, 6858–6860.
49 Y. Zhu, Y.-J. Ji, D.-G. Wang, Y. Zhang, H. Tang, X.-R. Jia, M. Song, G. Yu and G.-C. Kuang, *J. Mater. Chem. A*, 2017, **5**, 6622–6629.
50 T. R. Thomas, B. A. Staples, L. P. Murphy, Dry method for recycling iodine-loaded silver zeolite, *US Pat.* 4088737/A, 1978, **http://inis.iaea.org/search/search.aspx?orig_q=RN:10456359**.
51 J. A. Wang, K. L. Ai and L. H. Lu, *J. Mater. Chem. A*, 2019, **7**, 16850–16858.
52 A. J. Blake, F. A. Devillanova, R. O. Gould, W. S. Li, V. Lippolis, S. Parsons, C. Radek and M. Schroder, *Chem. Soc. Rev.*, 1998, **27**, 195–205.
53 X. Qian, Z. Q. Zhu, H. X. Sun, F. Ren, P. Mu, W. Liang, L. Chen and A. Li, *ACS Appl. Mater. Interfaces*, 2016, **8**, 21063–21069.

Open Access Article. Published on 24 2023. Downloaded on 23.04.26 04:24:07.
This article is licensed under a Creative Commons Attribution-NonCommercial 3.0 Unported Licence.

54 X. W. Pan, C. H. Ding, Z. M. Zhang, H. Z. Ke and G. E. Cheng, *Microporous Mesoporous Mater.*, 2020, **300**, 110161.
55 P. Chen, X. H. He, M. B. Pang, X. T. Dong, S. Zhao and W. Zhang, *ACS Appl. Mater. Interfaces*, 2020, **12**, 20429–20439.
56 T. H. Niu, C. C. Feng, C. Yao, W. Y. Yang and Y. H. Xu, *ACS Appl. Polym. Mater.*, 2021, **3**, 354–361.
57 P. Deplano, F. A. Devillanova, J. R. Ferraro, F. Isaia, V. Lippolis and M. L. Mercuri, *Appl. Spectrosc.*, 1992, **46**, 1625–1629.
58 N. S. Rao, G. B. Rao and D. Ziessow, *Spectrochim. Acta, Part A*, 1990, **46**, 1107–1124.
59 M. Hasani and M. Shamsipur, *J. Inclusion Phenom. Macrocyclic Chem.*, 2004, **48**, 135–139.
60 N. Alizadeh and A. Roomiani, *J. Chil. Chem. Soc.*, 2012, **57**, 1130–1133.
61 E. M. Nour, *Spectrochim. Acta, Part A*, 2000, **56**, 167–170.
62 X. Q. Yan, H. Wang, W. Di Chen and W. J. Jin, *Anal. Sci.*, 2014, **30**, 365–370.
63 T. M. Geng, S. N. Ye, Z. M. Zhu and W. Y. Zhang, *J. Mater. Chem. A*, 2018, **6**, 2808–2816.
64 A. Hijazi, B. Azambre, G. Finqueneisel, F. Vibert and J. L. Blin, *Microporous Mesoporous Mater.*, 2019, **288**, 109586.
65 S. Xiong, X. Tang, C. Pan, L. Li, J. Tang and G. Yu, *ACS Appl. Mater. Interfaces*, 2019, **11**, 27335–27342.
66 N. Liu, J. Chen, Z. Wu, P. Zhan, L. Zhang, Q. Wei, F. Wang and L. Shao, *ACS Appl. Polym. Mater.*, 2021, **3**, 2178–2188.
67 Z. J. Yan, B. Cui, T. Zhao, Y. F. Luo, H. C. Zhang, J. L. Xie, N. Li, N. S. Bu, Y. Yuan and L. X. Xia, *Molecules*, 2021, **26**, 5263.
68 X. H. Xu, Y. X. Li, L. Zhou, N. Liu and Z. Q. Wu, *Chem. Sci.*, 2022, **13**, 1111–1118.
69 B. Jiang, Y. Qi, X. F. Li, X. H. Guo, Z. M. Jia, J. Zhang, Y. Li and L. J. Ma, *Chin. Chem. Lett.*, 2022, **33**, 3556–3560.
70 K. C. Jie, Y. J. Zhou, E. R. Li, Z. T. Li, R. Zhao and F. H. Huang, *J. Am. Chem. Soc.*, 2017, **139**, 15320–15323.
71 C. C. Feng, G. J. Xu, W. Xie, S. R. Zhang, C. Yao and Y. H. Xu, *Polym. Chem.*, 2020, **11**, 2786–2790.
72 D. H. Dai, J. Yang, Y. C. Zou, J. R. Wu, L. L. Tan, Y. Wang, B. Li, T. Lu, B. Wang and Y. W. Yang, *Angew. Chem., Int. Ed.*, 2021, **60**, 8967–8975.
73 S. Y. Yao, W. H. Fang, Y. Y. Sun, S. T. Wang and J. Zhang, *J. Am. Chem. Soc.*, 2021, **143**, 2325–2330.
74 Z. J. Yan, Y. Yuan, Y. Y. Tian, D. M. Zhang and G. S. Zhu, *Angew. Chem., Int. Ed.*, 2015, **54**, 12733–12737.
75 J. T. Hughes, D. F. Sava, T. M. Nenoff and A. Navrotsky, *J. Am. Chem. Soc.*, 2013, **135**, 16256–16259.
76 D. F. Sava, M. A. Rodriguez, K. W. Chapman, P. J. Chupas, J. A. Greathouse, P. S. Crozier and T. M. Nenoff, *J. Am. Chem. Soc.*, 2011, **133**, 12398–12401.
77 B. J. Riley, J. Chun, W. Um, W. C. Lepry, J. Matyas, M. J. Olszta, X. H. Li, K. Polychronopoulou and M. G. Kanatzidis, *Environ. Sci. Technol.*, 2013, **47**, 7540–7547.
78 W. Zhang, Y. Mu, X. He, P. Chen, S. Zhao, C. Huang, Y. Wang and J. Chen, *Chem. Eng. J.*, 2020, **379**, 122365.
79 Y. Q. Hu, M. Q. Li, Y. Y. Wang, T. Zhang, P. Q. Liao, Z. P. Zheng, X. M. Chen and Y. Z. Zheng, *Chem.–Eur. J.*, 2017, **23**, 8409–8413.
80 H. C. Hu, F. Y. Chen, Z. Y. Zhang, D. C. Liu, Y. N. Liang and Z. L. Chen, *Front. Chem.*, 2022, **10**, 864131.
81 G. Brunet, D. A. Safin, M. Z. Aghaji, K. Robeyns, I. Korobkov, T. K. Woo and M. Murugesu, *Chem. Sci.*, 2017, **8**, 3171–3177.
82 Y. Z. Tang, H. L. Huang, J. Li, W. J. Xue and C. L. Zhong, *J. Mater. Chem. A*, 2019, **7**, 18324–18329.
83 C. Y. Yan and T. C. Mu, *Phys. Chem. Chem. Phys.*, 2014, **16**, 5071–5075.
84 Z. Zhang, X. Dong, J. Yin, Z. G. Li, X. Li, D. Zhang, T. Pan, Q. Lei, X. Liu, Y. Xie, F. Shui, J. Li, M. Yi, J. Yuan, Z. You, L. Zhang, J. Chang, H. Zhang, W. Li, Q. Fang, B. Li, X. H. Bu and Y. Han, *J. Am. Chem. Soc.*, 2022, **144**, 6821–6829.
85 J. H. Liu, Y. J. Qi, D. Zhao, H. H. Li and S. T. Zheng, *Inorg. Chem.*, 2019, **58**, 516–523.
86 S. Chibani, F. Chiter, L. Cantrel and J. F. Paul, *J. Phys. Chem. C*, 2017, **121**, 25283–25291.
87 D. Shetty, J. Raya, D. S. Han, Z. Asfari, J. C. Olsen and A. Trabolsi, *Chem. Mater.*, 2017, **29**, 8968–8972.
88 X. R. Zhang, I. da Silva, H. G. W. Godfrey, S. K. Callear, S. A. Sapchenko, Y. Q. Cheng, I. Vitorica-Yrezabal, M. D. Frogley, G. Cinque, C. C. Tang, C. Giacobbe, C. Dejoie, S. Rudic, A. J. Ramirez-Cuesta, M. A. Denecke, S. H. Yang and M. Schroder, *J. Am. Chem. Soc.*, 2017, **139**, 16289–16296.
89 B. F. Abrahams, M. Moylan, S. D. Orchard and R. Robson, *Angew. Chem., Int. Ed.*, 2003, **42**, 1848–1851.
90 A. Karhu, *Methods to prevent the source term of methyl iodide during a core melt accident*, Report No. NKS-13, ISBN 87-7893-063-4, VTT Energy, Finland, 1999.
91 S. H. Bruffey, R. T. Jubin and J. A. Jordan, Report No. FCRD-MRWFD-2016-000357; ORNL/TM-2016/568, 2016.
92 T. M. Nenoff, M. A. Rodriguez, N. R. Soelberg and K. W. Chapman, *Microporous Mesoporous Mater.*, 2014, **200**, 297–303.
93 B. Azambre, M. Chebbi and A. Hijazi, *Chem. Eng. J.*, 2020, **379**, 122308.
94 H. P. Zhang, L. L. Gong, M. J. Yin, X. H. Xiong, Q. Y. Zhang, X. F. Feng, F. Luo, J. B. Carney and Y. F. Yue, *Cell Rep. Phys. Sci.*, 2022, **3**, 100830.
95 B. Lee, D. Moon and J. Park, *Angew. Chem., Int. Ed. Engl.*, 2020, **59**, 13793–13799.
96 H. Chun, J. Kang and B. Han, *Phys. Chem. Chem. Phys.*, 2016, **18**, 32050–32056.
97 B. Y. Li, X. L. Dong, H. Wang, D. X. Ma, K. Tan, S. Jensen, B. J. Deibert, J. Butler, J. Cure, Z. Shi, T. Thonhauser, Y. J. Chabal, Y. Han and J. Li, *Nat. Commun.*, 2017, **8**, 485.
98 L. W. He, L. Chen, X. L. Dong, S. T. Zhang, M. X. Zhang, X. Dai, X. J. Liu, P. Lin, K. F. Li, C. L. Chen, T. T. Pan, F. Y. Ma, J. C. Chen, M. J. Yuan, Y. G. Zhang, L. Chen, R. H. Zhou, Y. Han, Z. F. Chai and S. Wang, *Chem*, 2021, **7**, 699–714.

 This journal is © The Royal Society of Chemistry 2023

Open Access Article. Published on 24 2023. Downloaded on 23.04.26 04:24:07.
This article is licensed under a Creative Commons Attribution-NonCommercial 3.0 Unported Licence.

99 Y. Q. Xie, T. T. Pan, Q. Lei, C. L. Chen, X. L. Dong, Y. Y. Yuan, W. Al Maksoud, L. Zhao, L. Cavallo, I. Pinnau and Y. Han, *Nat. Commun.*, 2022, **13**, 2878.
100 T. Brinck, J. S. Murray and P. Politzer, *Int. J. Quantum Chem.*, 1992, **44**, 57–64.
101 X. Y. Wu, L. J. Chen, E. J. Amigues, R. Y. Wang, Z. F. Pang and L. F. Ding, *Acs Omega*, 2021, **6**, 18169–18177.
102 A. M. S. Riel, R. K. Rowe, E. N. Ho, A. C. C. Carlsson, A. K. Rappe, O. B. Berryman and P. S. Ho, *Acc. Chem. Res.*, 2019, **52**, 2870–2880.
103 M. Chebbi, B. Azambre, C. Volkringer and T. Loiseau, *Microporous Mesoporous Mater.*, 2018, **259**, 244–254.
104 X. Guo, Y. Li, M. Zhang, K. Cao, Y. Tian, Y. Qi, S. Li, K. Li, X. Yu and L. Ma, *Angew. Chem., Int. Ed. Engl.*, 2020, **59**, 22697–22705.
105 Y. Z. Liao, J. Weber, B. M. Mills, Z. H. Ren and C. F. J. Faul, *Macromolecules*, 2016, **49**, 6322–6333.
106 Z. J. Yin, S. Q. Xu, T. G. Zhan, Q. Y. Qi, Z. Q. Wu and X. Zhao, *Chem. Commun.*, 2017, **53**, 7266–7269.
107 X. M. Li, G. Chen, J. T. Ma and Q. Jia, *Sep. Purif. Technol.*, 2019, **210**, 995–1000.
108 G. J. Xu, Y. Zhu, W. Xie, S. R. Zhang, C. Yao and Y. H. Xu, *Chem.–Asian J.*, 2019, **14**, 3259–3263.
109 L. Shao, N. Liu, L. Wang, Y. Sang, H. Wan, P. Zhan, L. Zhang, J. Huang and J. Chen, *Chemosphere*, 2022, **288**, 132499.
110 N. Soelberg and T. Watson, *FY-2016 methyl iodide higher NOx adsorption test report*, Report No. FCRD-MRWFD-2016-000352, INL/EXT-15-36817, Idaho National Laboratory, 2015.
111 Y. Q. Xie, T. T. Pan, Q. Lei, C. L. Chen, X. L. Dong, Y. Y. Yuan, J. Shen, Y. C. Cai, C. H. Zhou, I. Pinnau and Y. Han, *Angew. Chem., Int. Ed.*, 2021, **60**, 22432–22440.
112 S. Choi, Y. Nan and L. L. Tavlarides, *AIChE J.*, 2021, **67**(67), e17182.
113 B. Azambre, M. Chebbi, O. Leroy and L. Cantrel, *Ind. Eng. Chem. Res.*, 2018, **57**, 1468–1479.
114 S. U. Nandanwar, K. Coldsnow, M. Green, V. Utgikar, P. Sabharwall and D. E. Aston, *Chem. Eng. J.*, 2016, **287**, 593–601.
115 M. Chebbi, B. Azambre, C. Monsanglant-Louvet, B. Marcillaud, A. Roynette and L. Cantrel, *J. Hazard. Mater.*, 2021, **409**, 124947.
116 G. Y. Cha, S. E. Sivan, M. Lee, K. R. Oh, A. H. Valekar, M. K. Kim, H. Jung, D. Y. Hong and Y. K. Hwang, *J. Hazard. Mater.*, 2021, **417**, 125904.